On The Potential of InSAR for Estimating Crude Oil Volume Changes From the Deformation of Storage Tanks

Roland Akiki, Carlo de Franchis, Gabriele Facciolo, Raphaël Grandin, Jean-Michel Morel

ON THE POTENTIAL OF INSAR FOR ESTIMATING CRUDE OIL VOLUME CHANGES FROM THE DEFORMATION OF STORAGE TANKS

Roland Akiki [1,3] *Carlo de Franchis* [1,3] *Gabriele Facciolo* [1]
Raphaël Grandin [2] *Jean-Michel Morel* [1]

[1] Université Paris-Saclay, ENS Paris-Saclay, CNRS, Centre Borelli, 91190, Gif-sur-Yvette, France
[2] Institut de Physique du Globe de Paris, Université Paris VII, France
[3] Kayrros SAS

ABSTRACT

In this article, we examine the possibility of using the interferometric phase on some fixed corners of storage tanks to infer the tank fill ratio. For the study, we use floating roof tanks for which the fill ratio can be inferred from the floating roof position. We observe a correlation between the phase double difference taken at the fixed roof of neighboring tanks and the fill ratio double difference. We highlight some challenges that require further investigation and the development of adapted InSAR techniques.

***Index Terms*—** storage, tank, floating, fixed, roof, Persistent Scatterer, InSAR, SAR, oil, volume, deformation

1. INTRODUCTION

A *floating roof tank* is a storage medium typically used for volatile liquids, such as crude oil. In order to reduce evaporation loss, the roof on top of the tank moves vertically as the volume of liquid changes. Since these storage tanks often have large dimensions, they are often visible on images from Synthetic Aperture Radar (SAR) satellite constellations, such as COSMO-SkyMed, TerraSAR-X or Sentinel-1. As shown in Figure 1, we typically distinguish three bright pixels per tank in the amplitude of a SAR image in slant range geometry. They appear aligned on the same image row with increasing column index according to range (distance to the satellite):

(A) The corner formed between the platform on top of the tank and the tank façade, i.e., the fixed roof corner.
(B) The corner between the tank façade and its base, i.e., the fixed base corner.
(C) The corner between the inner wall of the tank and the horizontal floating roof, i.e., the floating roof corner.

When looking at a co-registered time series of SAR images, the fixed roof (A) and fixed base (B) corners remain in the same position. Conversely, the floating roof corner (C) moves by a few pixels from one date to another, corresponding to a height change.

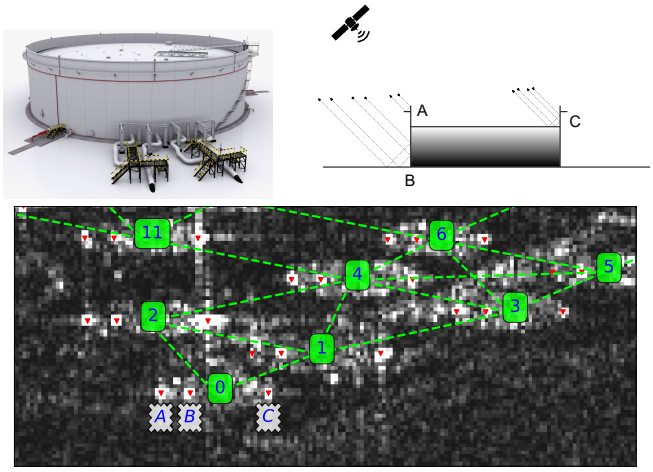

Fig. 1: SAR acquisition of storage tanks. On the top left is a 3D representation of a storage tank. In the top right, the three corners that exhibit strong reflections in a SAR image. On the bottom, a crop of a SAR amplitude image around some storage tanks for our area of interest. The tank ids and corner positions are displayed. We selected neighboring tanks according to the green connections.

In this article, our main contributions are:

- Establishing a correlation between Interferometric Synthetic Aperture Radar (InSAR) measurements on corners (A) and (B) and tank fill ratio measured using corner (C).

- Presenting a novel InSAR use case which could motivate the development of adapted InSAR techniques.

Work financed by a grant from ANRT N° 2019/2003. Work partly financed by Office of Naval research grant N00014-20-S-B001. Centre Borelli is also a member of Université Paris Cité, SSA and INSERM.

2. RELATED WORK

Several methods [1, 2] were previously developed to convert the floating roof corner (C) column index at a certain date into a crude oil volume (or a normalized "fill ratio" $\in [0, 1]$) for the storage tank. On the other hand, InSAR techniques have demonstrated their accuracy in estimating millimetric surface deformation by comparing the phase of Single Look Complex (SLC) SAR images. Recently, InSAR was applied to a pair of Sentinel-1 images of storage tanks to study the potential of the technique in assessing the health and stability of these structures [3]. Also, relevant to this work, advanced InSAR algorithms were developed throughout the years [4]. Among those, we distinguish the approach which restricts the analysis to a group of stable reflectors with high Signal-to-Noise Ratio (SNR), called Persistent Scatterers (PS) [5, 6]. More precisely, the technique is performed on a time series of SAR images. The simplest metric to evaluate the stability of the scatterer in the PS technique is the amplitude dispersion index, given by

$$D_{\mathcal{A}}(Q) = \frac{\sigma_{\mathcal{A}}(Q)}{m_{\mathcal{A}}(Q)}, \tag{1}$$

where $m_{\mathcal{A}}$ and $\sigma_{\mathcal{A}}$ are the mean and the standard deviation of the amplitude values taken along the time series for any point Q in the image. The amplitude dispersion is an indicator of the phase stability, at least for high SNR values [5] (lower $D_{\mathcal{A}}$ means better stability). Therefore, a point Q in the image is selected as a PS if $D_{\mathcal{A}}(\mathrm{Q}) < \tau$, where τ is a threshold (usually around 0.25).

Furthermore, the phase double difference on reflectors p and q for images i and j is defined as

$$\Delta\Phi_{i,j}(p,q) = \angle\left[(z_i(p)\cdot z_j(p)^*)\cdot(z_i(q)\cdot z_j(q)^*)^*\right], \tag{2}$$

where $z_i(p)$ is the complex number for image i at reflector p, * denotes the conjugation operation, and $\angle$ is the observed angle $\in [-\pi, \pi)$. During PS processing, $\Delta\Phi_{i,j}(p,q)$ is estimated on two nearby PS reflectors to mitigate the atmospheric effects.

We test the same strategy to derive InSAR measurements between fixed reflectors on the tanks. We can expect that the deformation of the tank will be the predominant signal in the phase double difference. Other noteworthy effects that could have a meaningful impact on the phase double difference are the residual topographic error phase, the noise and the phase wrapping. Nevertheless, we hope to measure small millimetric movements of the fixed reflectors between two dates, which may indicate crude oil volume change.

3. EXPERIMENTS

Our Area Of Interest (AOI) contains $N_T = 19$ tanks in the Juaymah tank farm in Saudi Arabia (lon=49.987°, lat=26.819°). We selected Sentinel-1 relative orbit 101 and dates from 2017-01-05 to 2021-12-22, resulting in $N_I = 151$ images. We selected the first date as the primary image

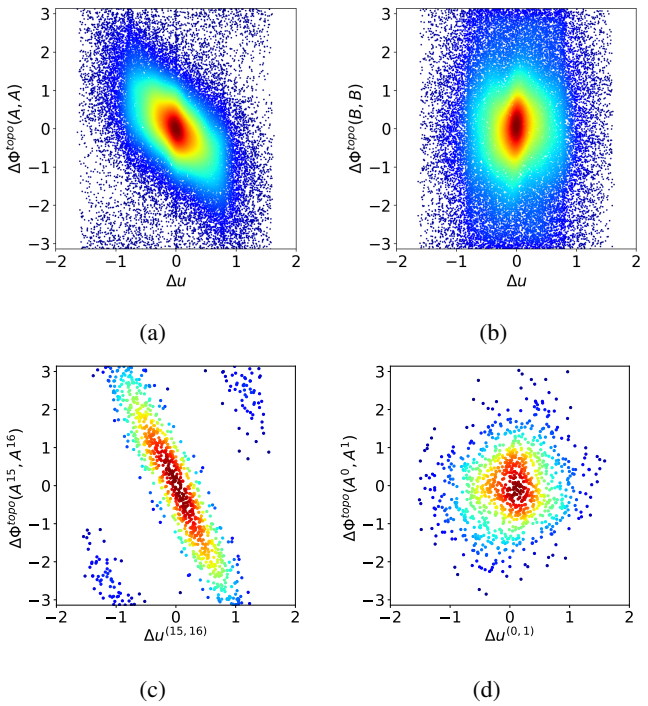

Fig. 2: Scatterplots obtained for the phase double difference against the fill ratio double difference between neighboring tanks. The color indicates increasing point density from blue to red obtained using Gaussian kernel density estimation. Figures 2a and 2b correspond to taking all tank couples at the roof and base, respectively. We see a trend in the roof and no trend in the base. For the last two plots, we show tank couple (15, 16) that exhibits good linear behavior (2c) and tank couple (0,1) with no visible correlation (2d).

and generated co-registered crops of size 512×1024 pixels around our AOI using a procedure based on the geolocation of a set of points sampled on the Shuttle Radar Topography Mission (SRTM) Digital Elevation Model (DEM) [7]. We also estimated an orbital phase ϕ^{orb} and a topographic phase ϕ^{topo} per image (relative to the primary image) such that the compensation operation is given by $z_i^{orb}(p) = z_i(p)\cdot \mathrm{e}^{j\phi_i^{orb}(p)}$ and $z_i^{topo}(p) = z_i^{orb}(p)\cdot \mathrm{e}^{j\phi_i^{topo}(p)}$. Consequently, phase double differences $\Delta\Phi_{i,j}^{orb}(p,q)$ and $\Delta\Phi_{i,j}^{topo}(p,q)$ can be defined according to Equation 2.

Since the floating roof may move by several meters between acquisitions, the phase double difference using (C) is affected by phase ambiguity (2π cycle is 2.8 cm for Sentinel-1), hence unusable for interferometry. Instead, we attempt to derive a proxy of the tank fill ratio by analyzing the phase double difference using corners (A) and (B). Although corners (A) and (B) are at first order fixed, they may be subject to relative displacement due to tank deformation, presumably resulting indirectly from filling. An estimation of the fill ratio for each tank k and each image i, $u_i^k \in [0, 1]$, was provided by

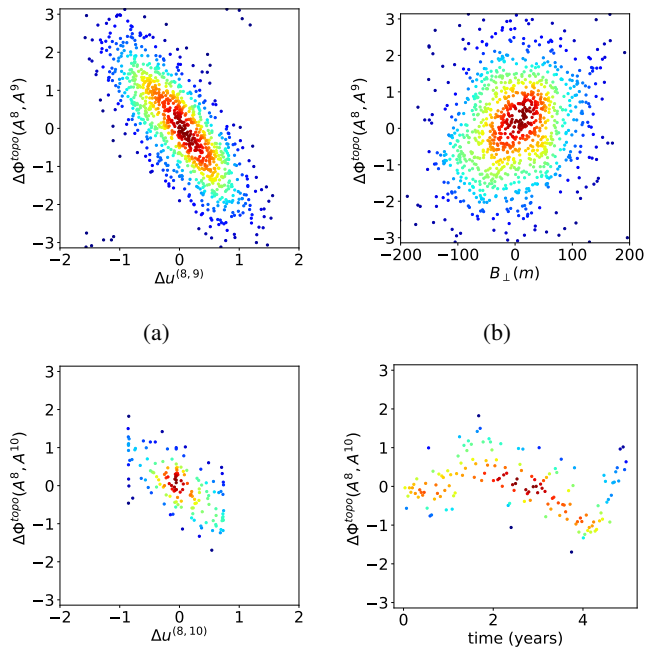

Fig. 3: Scatterplots highlighting the presence of uncompensated effects in the phase. The phase double difference on the roof of tank couple (8, 9) vs. the fill ratio double difference (3a), and vs. the perpendicular baseline (3b). For the last two plots, all interferograms are done w.r.t. the first date and the scatterplots were recentered by removing the bias induced by the first date for visualization purposes. We see the phase double difference on tank couple (8, 10) vs. the fill ratio double difference (3c) and vs. the temporal baseline (3d).

Kayrros [1]. We define the fill ratio double difference between two tanks and two dates as

$$\Delta u_{i,j}^{k,l} = (u_i^k - u_j^k) - (u_i^l - u_j^l), \quad \Delta u_{i,j}^{k,l} \in [-2, 2]\,. \quad (3)$$

We define A^k and B^k the fixed roof and fixed base corners of the tank k respectively, with $k \in \{0 \dots N_T - 1\}$. We compared the values of $\Delta\Phi_{i,j}^{topo}\left(X^k, X^l\right)$ against the fill ratio double difference $\Delta u_{i,j}^{k,l}$, where X can be either A or B.

The experiments were conducted on the set of neighboring tanks $T = \{(k,l) \mid \text{distance}(k,l) < \tau_{dist}\}$ as seen in the bottom image of Figure 1 (here $\tau_{dist} = 300$ m). The images were also selected from the set $S = \{(i,j) \mid \text{duration}(i,j) < \tau_{temp}\}$ (here $\tau_{temp} = 90$ days). The results can be seen in Figure 2. In Figure 2a, the phase double difference is taken on the roof for all tank couples in T and all image couples in S. When the roof corners A^k are considered, a trend suggesting a negative correlation between the two quantities is visible in approximately half of the tank couples, e.g. couple (A^{15}, A^{16}) shown in Figure 2c. The plot suggests that the phase double difference is mostly already unwrapped

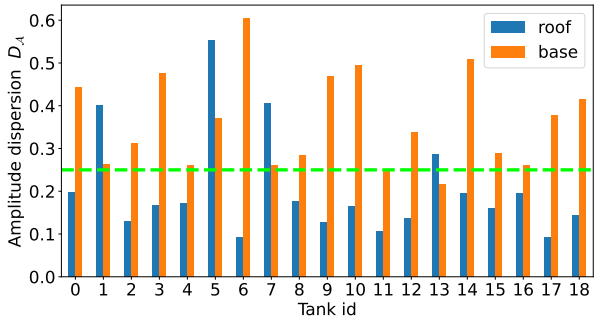

Fig. 4: The measured amplitude dispersion for all tank ids at the fixed roof (A) in blue, and at the fixed base (B) in orange. The dashed green line indicates the threshold 0.25, usually used to detect stable reflectors in the PS technique.

since wrapping occurs on a limited set of points with the biggest absolute values of the fill ratio double difference. Therefore a tank filling up induces a fixed roof movement away from the satellite in the order of 1 cm. This relationship is not verified for the other half of tank couples, e.g. couple (A^0, A^1) in Figure 2d. Furthermore, Figure 2b shows that no clear trend emerges when using the fixed base reflectors.

On the other hand, Figure 3 shows the presence of some uncompensated factors affecting the phase. Indeed, we observe a dependence of the phase double difference on the orthogonal baseline for some tank couples, as can be seen in Figure 3b for the couple (A^8, A^9). This indicates that there is an uncompensated topographic term due to inaccuracies in the simulated topographic phase ϕ^{topo}. Furthermore, we also observe an occasional dependence on time, as can be seen in Figure 3d for couple (A^8, A^{10}). Note that for this plot, all interferograms are computed with respect to the first image in order to be able to show the evolution with time, i.e only for Figures 3c and 3d, the set S of image couples is selected as $S = \{(0,j) \mid j = 1 \cdots N_I - 1\}$.

Moreover, we notice that the noise in the scatterplots increases when the corner is not a persistent scatterer, according to the traditional amplitude dispersion metric $D_\mathcal{A}$. We compute this metric on the roofs and bases of the tanks, $D_\mathcal{A}(A^k)$ and $D_\mathcal{A}(B^k)$ respectively, for $k = \{0 \cdots N_T - 1\}$. From Figure 4, we can make two observations:

- The amplitude dispersion of the base is globally higher than the amplitude dispersion of the roof (the value at the base is higher than the threshold of 0.25 for most of the tanks).

- The amplitude dispersion might indicate which scatterplots will be noisier. For instance, point A^1 for which the amplitude dispersion is high ($D_\mathcal{A}(A^1) = 0.4$), is probably responsible for the noise seen in the scatterplot for couple (A^0, A^1) in Figure 2d, whereas a trend can be seen in Figures 2c, 3a, 3c, for corners

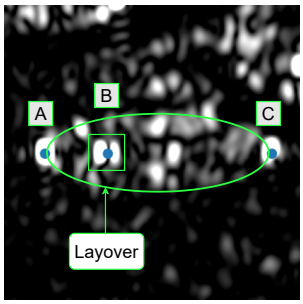

(a)

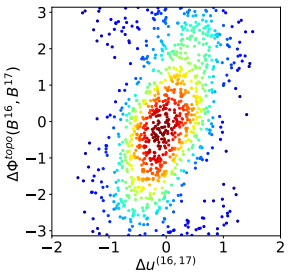

(b)

Fig. 5: Base reflector behaviour. On the left is a zoomed image of the tank 0. We clearly see the layover effect from the floating roof affecting the base and drowning it in clutter. On the right, we see a trend for tank couple (16, 17) between the phase double difference at the base and the fill ratio double difference.

$(A^8, A^9, A^{10}, A^{15}, A^{16})$ which have low $D_{\mathcal{A}}$.

Finally, let us focus on the base corners (B). We already established that no clear trend emerges in Figure 2b, and that most amplitude dispersions are high. From Figure 5a, we see that this may be caused by the small reflections from the top of the floating roof, which often contaminate the base and drown it in clutter because of the layover effect. This phenomenon is emphasized by the fact that the tank is full at this date. However, a trend still sometimes emerges for some tank couples at the base, as can be seen in Figure 5b.

4. CONCLUSION

In this study, we examined the relationship between the InSAR measurements on the fixed corners of floating roof storage tanks and the tank fill ratio inferred from the floating roof. We conclude that we sometimes observe a correlation between the fill ratio double difference and the phase double difference, mainly at the fixed roof corner of the tank. The trend suggests that a tank filling up induces a movement of the fixed roof corner away from the satellite in the order of 1 cm. On the other hand, some effects related to the residual topographic phase and some slow temporal trends may also be present. Furthermore, the noise level in the scatterplots is related to the amplitude dispersion index of the reflectors involved. In other words, unstable reflectors according to traditional metrics are less likely to exhibit visually compelling trends. Generally speaking, phase measurements from the fixed base reflector are noisy. We posit that this is due to the layover effect of the floating roof. Nonetheless, we can see some correlation between the phase and fill ratio double differences for some tank couples at the base.

All those challenges listed suggest the need to develop further adapted InSAR techniques to this specific use case. However, the experiments conducted on floating roof tanks are encouraging. In the future, by developing a method to infer a tank fill ratio from InSAR measurements, one could attempt to apply the same methodology on fixed roof tanks. It would then be possible to measure the fixed roof tank fill ratio from the small millimetric deformations of its fixed corners.

5. REFERENCES

[1] Carlo De Franchis, Guillaume Lostis, Hefdhi Abdennadher, Pablo Arias, Thomas Madaule, Axel Davy, Sylvain Calisti, Jean-Michel Morel, Raffaele Grompone, and Gabriele Facciolo, "Method and system for remotely measuring the volume of liquid stored in external floating roof tanks," June 2 2020, US Patent 10,672,139.

[2] Carlos Villamil Lopez and Uwe Stilla, "Monitoring of Oil Tank Filling with Spaceborne SAR Using Coherent Scatterers," *IEEE Journal of Selected Topics in Applied Earth Observations and Remote Sensing*, vol. 14, pp. 5638–5655, 2021.

[3] Geoffrey O. Nwodo, Francis I. Okeke, and Nixon N Nduji, "Application of Interferometric Synthetic Aperture Radar (InSAR) Technique in Monitoring the Deformation of Large Oil Storage Tanks," *World Journal of Research and Review*, vol. 15, no. 6, pp. 18–25, 2022.

[4] Dinh Ho Tong Minh, Ramon Hanssen, and Fabio Rocca, "Radar interferometry: 20 years of development in time series techniques and future perspectives," *Remote Sensing*, vol. 12, no. 9, pp. 1364, 2020.

[5] Alessandro Ferretti, Claudio Prati, and Fabio Rocca, "Permanent scatterers in SAR interferometry," *IEEE Transactions on Geoscience and Remote Sensing*, vol. 39, no. 1, pp. 8–20, 2001.

[6] Alessandro Ferretti, Claudio Prati, and Fabio Rocca, "Nonlinear subsidence rate estimation using permanent scatterers in differential SAR interferometry," *IEEE Transactions on Geoscience and Remote Sensing*, vol. 38, no. 5 I, pp. 2202–2212, 2000.

[7] Roland Akiki, Jérémy Anger, Carlo de Franchis, Gabriele Facciolo, Jean-Michel Morel, and Raphaël Grandin, "Improved sentinel-1 iw burst stitching through geolocation error correction considerations," in *IGARSS 2022 IEEE International Geoscience and Remote Sensing Symposium*. IEEE, 2022, pp. 3404–3407.